doi.org/10.15392/2319-0612.2025.2866
Braz. J. Radiat. Sci., Rio de Janeiro
2025, 13(3) | 01-33 | e2866
Submitted: 2025-02-24
Accepted:2025-05-19

Implementation of automation tools for test analysis in the Radiotherapy Quality Assurance Programs

Santiago [a*], J. G. R.; Furnari [b], L.; Rodrigues [b], M. V. S. P.; Ribeiro [b], V. A. B.

[a] Faculdade de Medicina Universidade de São Paulo, 05403-000, São Paulo - SP, Brazil
[b] Serviço de Radioterapia, Hospital das Clínicas HCFMUSP, 05403-900, São Paulo - SP, Brazil.

*Correspondence: joaogrsantiago@gmail.com

Abstract: The increasing complexity of techniques used in radiotherapy demands a quality assurance program that evolves to ensure efficient quality control of equipment and associated devices. Many periodic tests rely on analyzing acquired images, typically compared to predefined standards to verify consistancy—checks that can often be automated. Automated analyses enable greater standardization, reduced subjectivity, improved accuracy, and shorter quality control times. To implement such tools, it is essential to assess factors such as accuracy, error detection sensitivity, adaptability to institution needs, and ease of access and use for those involved in quality control processes. This study evaluated two automation tool interfaces: the commercial SunCHECK Machine by Sun Nuclear® and a web application implementing modules from the open-source Pylinac library. Both interfaces were suitable to the quality assurance program, using coherent methodologies to calculate key metrics outlined in reference documents. Each tool has unique features and specific considerations, highlighted throughout the study based on evaluating Picket Fence, Star Shot, Winston-Lutz tests, field analysis, and Cone Beam Computed Tomography image quality. The findings highlight the importance of conducting studies during the implementation phase of such tools to understand the algorithms used and establish appropriate usage and control measures for routine practice. Both interfaces proved capable of quantifying the relevant quantities based on the reference documents, providing more efficient and effective quality control.

Keywords: Radiotherapy, Quality Assurance, Pylinac, SunCHECK Machine.

doi.org/10.15392/2319-0612.2025.2866
Braz. J. Radiat. Sci., Rio de Janeiro
2025, 13(3) | 01-33 | e2866
Submitted: 2025-02-24
Accepted:2025-05-19

Implementação de ferramentas de automatização para análise de testes no Programa da Garantia da Qualidade em Radioterapia

Resumo: O aumento crescente da complexidade das técnicas utilizadas na radioterapia exige um eficiente programa de garantia de qualidade que acompanhe essa tendência, de forma a garantir um controle da qualidade do aparelho e dispositivos associados. Muitos testes periódicos são baseados na análise de imagens adquiridas, e geralmente existem padrões aos quais essas imagens são comparadas para verificar sua constância, verificações essas passíveis de automatização. As análises automatizadas possibilitam uma maior padronização, redução da subjetividade, precisão e redução no tempo requerido para o controle da qualidade. Para a implementação de tais ferramentas é necessário avaliar fatores como precisão, sensibilidade na identificação de erros, adaptação às necessidades da instituição, e facilidade de acesso e de uso para aqueles que participam dos processos de controle da qualidade. Neste trabalho foram avaliadas duas interfaces de ferramentas de automatização, a comercial SunCHECK Machine® da Sun Nuclear, e um web aplicativo implementado contendo os módulos da biblioteca aberta *Pylinac*. Ambas as interfaces de avaliação se mostraram aplicáveis no programa de garantia da qualidade, calculando com metodologias coerentes as grandezas de interesse apresentadas nos documentos referência. Cada uma apresenta suas peculiaridades e áreas de atenção, que são destacadas ao decorrer do trabalho, a partir da avaliação dos testes de *Picket Fence*, *Star Shot*, *Winston-Lutz*, análise de campo radioativo, e qualidade da imagem do *Cone Beam Computed Tomography*. Com isso nota-se a importância da condução de estudos na fase de implementação de tais ferramentas, com intuito de promover o entendimento dos algoritmos utilizados, e estabelecer a forma de utilização e os controles necessários na rotina. Ambas as interfaces se mostraram capazes de quantificar as grandezas relevantes com base nos documentos de referência, propiciando um controle da qualidade mais eficiente e eficaz.

Palavras-chave: Radioterapia, Garantia da Qualidade, *Pylinac,* SunCHECK Machine.

1. INTRODUCTION

The objective of any quality assurance (QA) is to ensure that the performance and characteristics of the machine, associated devices, and processes do not significantly deviate from the values established during the acceptance and commissioning phase [1-2]. The increasing complexity of planning and treatment techniques in radiotherapy also demands a more efficient, safe, and effective QA [3-4]. In this context, many periodic tests that rely on image analysis, ranging from isocenter verification [5-6] and multileaf collimator (MLC) performance [7-8] to image quality evaluation for image-guided radiotherapy (IGRT) [9], can be automated either partially or entirely.

Several automation implementations are already commercially available and demonstrate significant advantages in their applicability, reducing both the time required and operator-dependent variability [10-12]. However, acquiring these solutions may involve high costs depending on the economic context of the institution. Alternatively, fully developing in-house tools can be a viable solution, but medical physicists often lack the necessary robust training in programming and data science. In this regard, open-source libraries such as Pylinac, as they enable automated image analysis with just a few lines of code and offering multiple modules for various tests commonly used in radiotherapy quality control [13].

Despite the great potential of these tools, careful analysis must be conducted before any implementation in clinical routine to ensure that the parameters tested in automated analysis align with those established in reference documents [14-16]. Thus, this study compares two tools for automating QA machine tests: the commercial platform SunCHECK® Machine (SCM) and an interface built using Pylinac's open-source modules. This work does not intend to provide a rigorous quantitative analysis of the evaluated tools, given the limited dataset available from the machine on which the tests were conducted. Instead, a qualitative analysis

is presented, focusing on the relationship between the obtained measurements and those defined in the reference documents, as well as the analysis methodologies, functionalities, and feasibility of implementing each interface within the QA program.

2. MATERIAL AND METHODS

This study was conducted using images acquired from the TrueBeam® (Varian Medical Systems, Palo Alto, USA) linear accelerator available at the Institute of Radiology (INRAD) of the Hospital das Clínicas da Faculdade de Medicina da Universidade de São Paulo (HCFMUSP). The machine is equipped with a Millennium® HD 120 MLC collimator, consisting of leaves that are 0.25 cm wide in the central 8 cm and 0.5 cm wide in the periphery, with a maximum field size of 22 cm.

The tests performed for evaluation included the Picket Fence, Star Shot, and Winston-Lutz tests, as well as the analysis of the radiation field and Cone Beam Computed Tomography (CBCT) image quality. MV images were acquired using a high-energy beam (6 MV with a flattening filter), while kV-CBCT images were obtained using a kilovoltage beam with a specific protocol. The detailed methodology for image acquisition for each test is described in the following sections.

The test tolerances were determined based on AAPM reports, primarily Hanley et al. (*Task Group 198*, 2021) [15], which provides updates and a guide for implementing the recommendations of Klein *et al.* (*Task Group 142*, 2009) [1] regarding quality assurance.

2.1. Data Aquisition

2.1.1. Picket Fence Aquisition

For the acquisition of the Picket Fence test image, the MV imaging panel, EPID (Electronic Portal Imaging Device), was positioned at a source-to-image distance (SID) of 100

cm, with the lateral and longitudinal positions centered. Irradiation was performed using a dynamic arc, with the gantry starting at 179° and rotating counterclockwise to 187°, delivering 480 MU. The acquired image, containing the 10 picket patterns with a leaf gap of 1.5 mm, formed by the movement of the MLC during the arc delivery, is presented in Figure 1.

Figure 1: Picket fence image pattern acquired in arc delivery

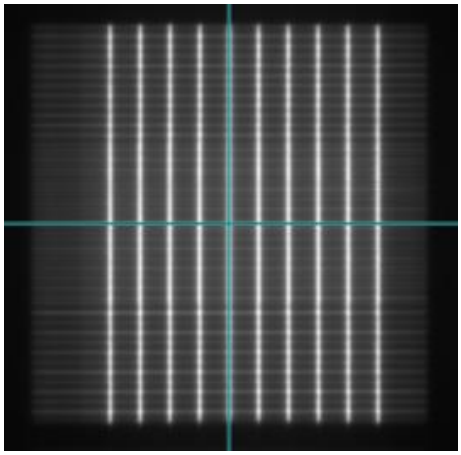

2.1.2. Star Shot Aquisition

Irradiation of the characteristic star pattern for the Star Shot test was performed using narrow geometry fields, spoke shots, with a size of 0.6 × 10.0 cm² (x, y). For the evaluation of the collimator isocenter, the EPID was used with a SID of 100 cm, and images were acquired at angles of 0°, 30°, 60°, 270°, and 315°. For the evaluation of the gantry isocenter and the table isocenter, an image plate (IP) model PC Type C® (Fujfilm, Tokyo, Japan) was used. In each case, the IP was properly aligned using the lasers: positioned vertically along the axial direction for the gantry test and horizontally, perpendicular to the beam axis, for the table test (Figure 2).

Figure 2: IP setup in the Star Shot acquisition: a) Gantry test; b) Table test.

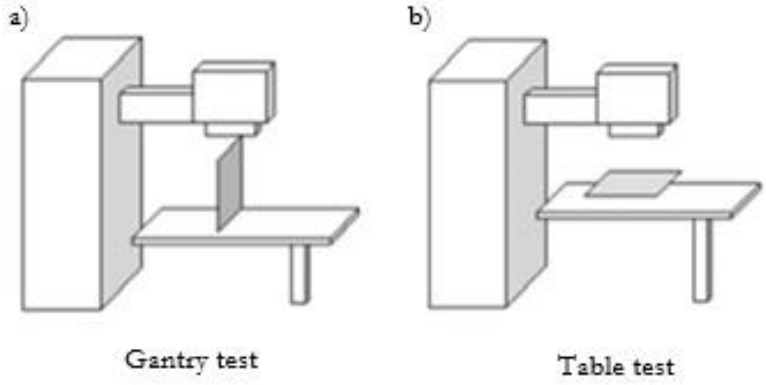

The gantry angles used for irradiation were 0°, 70°, 140°, 220°, and 290°, while the table angles were 0°, 45°, 90°, 300°, and 330°.

2.1.3. Winston-Lutz Aquisition

For the acquisition of Winston-Lutz test images, the MultiMet-WL® (Sun Nulclear, Melbourne, FL, USA) phantom was positioned using lasers and the light field reticle, based on the mechanical isocenter position. The central beam axis was aligned with the isocenter marker sphere of the phantom, which is made of tungsten and has a diameter of 5 mm (Figure 3).

Figure 3: Setup for the acquisition of the Winston-Lutz test with the MultiMet-WL®

The field size used was 2.2 × 2.5 cm² (x, y) delivering 20 MU, irradiated at the gantry, collimator, and table positions described in Table 1. Images were acquired using EPID with a SID of 150 cm.

Table 1: Field geometry in Winston-Lutz test.

Field ID	*Gantry* (°)	Collimator (°)	Couch (°)
WL1	0	0	0
WL2	0	270	0
WL3	0	315	0
WL4	0	90	0
WL5	0	45	0
WL6	180	0	0
WL7	90	0	0
WL8	270	0	0
WL9	0	0	90
WL10	0	0	45
WL11	0	0	270
WL12	0	0	315

2.1.4. Radiation Field Aquisition

For the acquisition of the radiation field, the collimators defined a 10 × 10 cm² field, with the EPID exposed at a SID of 150 cm. A sheet of graph paper with a centrally positioned radiopaque spherical marker was placed on the treatment table, aligned with the reticle. This setup allowed visualization of the center of the light field and comparison with the size of the radiation field. The field was irradiated with 10 MU, and its image can be seen in Figure 4.

Figure 4: Radiation field 10x10 cm² acquired. Note the radiopaque marker, positioned in the center of the light field, indicated by the arrow.

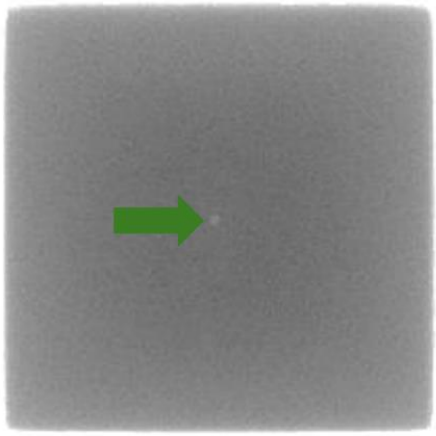

2.1.5. CBCT Aquisition

For the analysis of kV-CBCT image quality, the Catphan® 604 (The Phantom Laboratory, Salem, NY, USA) phantom was used, which contains modules for evaluating uniformity, geometric distortion, contrast, noise, spatial resolution, and slice thickness, which can be seen in Figure 5.

Figure 5: On the left, each of the scan sctions, acquired in the image. On the right, the location of each section in the phantom [17]

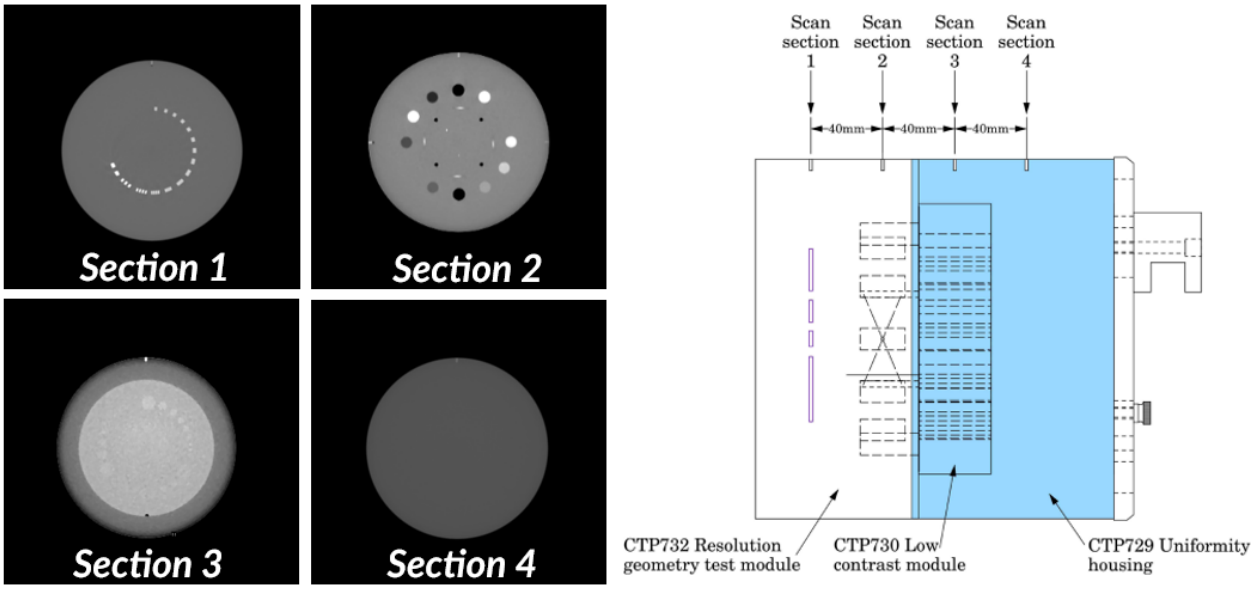

The phantom was positioned on the edge of the accelerator table using its own case for support, ensuring proper alignment and leveling. Longitudinally, it was positioned at the scan section 2, to ensure it was fully encompassed by the CBCT scan. The protocol selected for this study was the Pelvis protocol, with 125 kV, 1080 mAs, a half-fan beam mode, and a full-arc trajectory. The reconstruction algorithm used was iCBCT [18], with a slice thickness of 2 mm, resulting in a total of 89 images.

2.2. Image Analysys Methodology

The image analysis was conducted using two approaches: the SunCHECK® Machine (SCM, Sun Nulclear, Melbourne, FL, USA) platform (V.4.3.3) [19], and a custom interface developed using Pylinac (V.3.38) in Python [13].

SCM is a commercial platform by Sun Nuclear that efficiently automates image and log data collection, processing, and analysis. The platform is accessed via a web browser and includes pre-configured test templates compliant with Report of AAPM Task Group 142 [1], while also allowing customization according to the institution's specific needs.

Pylinac is an open-source Python library that provides multiple automated image analysis modules for quality control in radiotherapy. In combination with the Streamlit library [20] (V.1.37) open-source Python framework, which facilitates the development of interactive web applications, a custom interface was created containing the necessary modules for analyzing the selected test images.

The following sections briefly explore the reasoning behind the algorithms used for analysis, highlighting the differences in calculation methodologies between the two evaluated tools.

2.2.1. Picket Fence Analysis

In the SCM platform, the analysis of the Picket Fence test is based on the Mamalui-Hunter formalism [21]. First, the image is registered, adjusting its center and rotation if

necessary. After that, the algorithm identifies the irradiated stripes by generating the average profile along lines perpendicular to the movement of the leaves, obtaining a profile as shown in Figure 6.

Figure 6: Average rectangular profile in the horizontal direction of the Picket Fence test image.

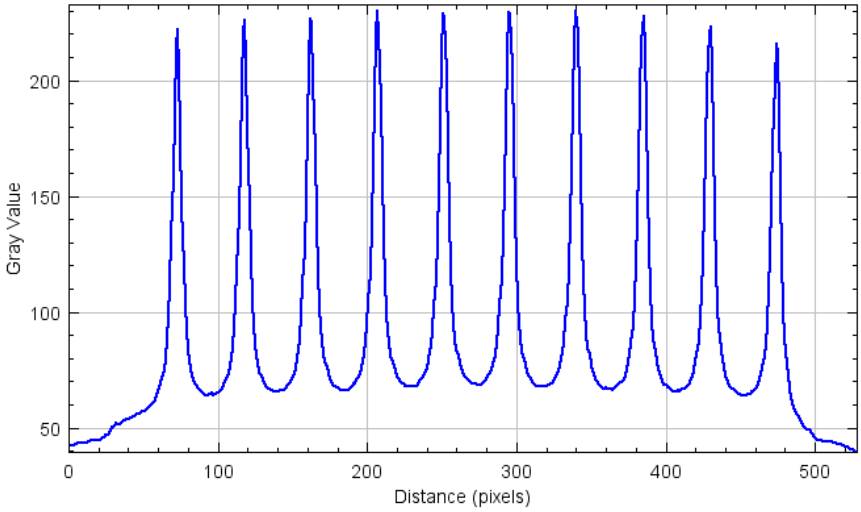

Next, for each horizontal line corresponding to a MLC pair, a Gaussian or Lorentzian curve is fitted to describe the peak of each stripe. Then, for each line, that corresponds to a pair of leafs, the difference between the center position of the Gaussian (found leaf pair position) and the central position of the stripe determined by a linear fit of the average rectangular profile (expected position), is computed (Figure 7). This difference is then compared to the established tolerance. Additionally, the curve data allow measurement of the stripe width.

The Pylinac Picket Fence module enables analysis based on either individual leaf detection or a combined approach, similar to SCM. Since leaf pairs have historically been evaluated together in automated methods, the combined approach was selected for comparative purposes. Moreover, the algorithm used in the combined method is similar to the one implemented in SCM, with the exception that the peak position used for comparison with the ideal position is determined at the center of full width at half maximum (FWHM).

Additionally, the Pylinac analysis also provides the angle of the leaves, which corresponds to the closest value to the cardinal direction.

Figure 7: Picket Fence test leaf pair positions identified by the algorithm. The dashed green line shows the expected position of the fit for the picket; the green band, the tolerance margin around the expected position; the blue lines the center of the gap of each identified leaf pair that is within tolerance of the expected position, and red those that exceed it.

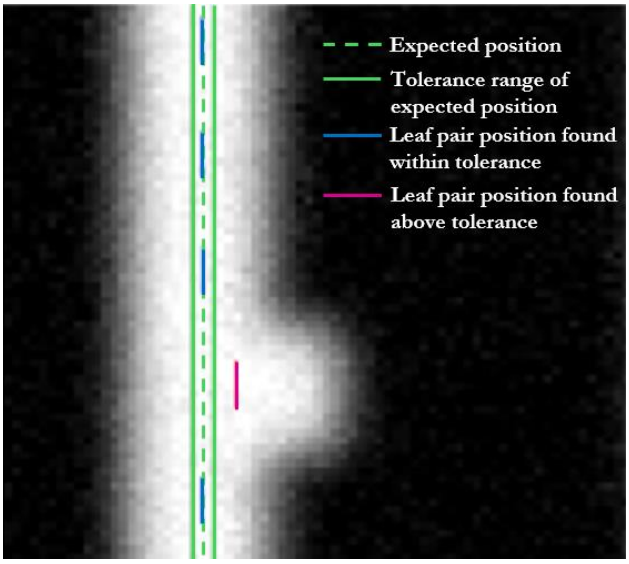

2.2.2. Star Shot Analysis

In general, most automated analysis tools for the Star Shot test are based on the concept of determining the minimum inscribed circle in the star pattern, as proposed by Gonzalez [22] e Depuydt [23]. The main difference between the SCM implementation and the Pylinac Star Shot module lies in how each method identifies the center of the irradiated beams while minimizing bias due to small noise variations or maximum grayscale values in pixel intensity.

In SCM, the algorithm sets a grayscale threshold to distinguish the spokes (the superposition of the radiative marks of the fields), from the image background and defines a search circle. In the grayscale profile along this circle, the spokes are identified as continuous arc segments where the values exceed the predetermined threshold. Each spoke is then assigned to the center of these segments and subsequently paired. If all spokes are not correctly identified, the threshold value and circle center can be manually adjusted. In

Pylinac, a circular grayscale profile is extracted from the image, peaks are identified, and spokes are determined by the center of the FWHM around these peaks. If spoke identification is inaccurate, the radius of the circular sampling profile can be adjusted; in this study, a radius equal to 50% of the smallest image dimension was adopted. Once the opposing spokes are identified and paired, both implementations apply an optimization algorithm to determine the diameter of the minimum enclosing circle for the central irradiated lines.

2.2.3. Winston-Lutz Analysis

For the analysis of the Winston-Lutz test, both implementations (SCM and Pylinac) begin similarly. First, in each image, the central axis (CAX) of the field is detected based on edge detection and the calculation of its center of mass. Both tools can perform this step for both rectangular and circular fields. Next, the edges of the radiopaque sphere in the phantom are identified by determining an optimal grayscale threshold for its detection and calculating its center of mass based on its radius. As a result, in each image, the vector associated with the displacement between these two centers are obtained, computing the maximum observed deviation. Subsequently, the mathematical formalism presented by Low [24] is applied, where geometric transformations are used to convert 2D coordinate deviations into 3D vector displacements. This also allows determining the optimal shift to apply to the phantom to minimize the maximum error.

Differences between the two tools emerge in the additional results and applied methodologies. In Pylinac, based on Winkler's findings [25], the gantry isocenter is calculated using the sphere's center as a fixed reference point (excluding images with nonzero table angles). A back-projection algorithm reconstructs the CAX trajectory in 3D space, determining its center and size. The collimator isocenter (in the plane normal to the gantry) and the table isocenter (in the coronal plane) are also calculated based on the maximum distances found between any two CAX positions and any two sphere centers, respectively.

Additionally, Pylinac enables the generation of error plots concerning gantry, collimator, table, and EPID positions individually, as well as a visualization plot of the calculated isocenters. Using the displacement coordinates that minimize errors, a virtual shift can be simulated, calculating the expected errors if the displacement were applied and the images were acquired again (Figure 8).

Figure 8: Isocenter visualization calculated in Winston-Lutz Pylinac's module. The image on the left refers to the visualization based on the original images, and the right is based on the simulation of the visualization that would be obtained by applying the optimal shift.

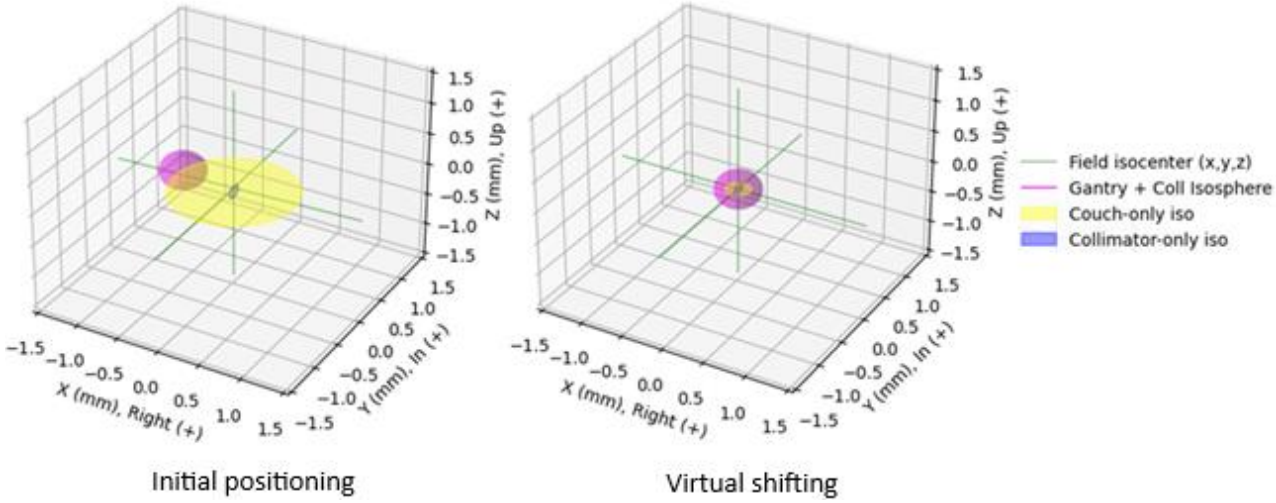

In SCM, the gantry isocenter is estimated solely based on the maximum deviation due to the gantry in each direction. The Hancock Winston-Lutz tool provides additional analyses based on the test interpretations described in Hancock's paper [26]. In this case, the diameter of the table isocenter is also calculated, along with its coronal plane distance from the phantom sphere position and the gantry isocenter. Additionally, the 2D couch results are simulated under the assumption that the optimal displacement was applied (Figure 9). Furthermore, diagrams related to gantry sag and errors associated with beam steering are also computed.

Figure 9: Visualization of the sphere positions based on the images with couch angle in the SCM. On the left, deviations obtained with the initial image, and on the right, that would be obtained by applying the optimal shift.

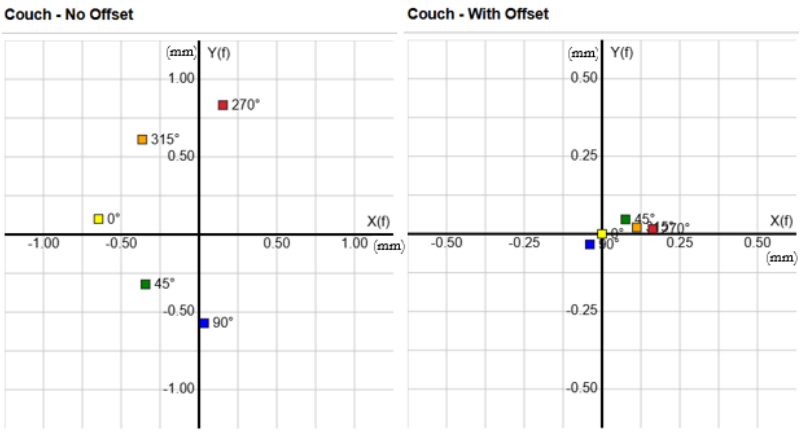

2.2.4. Radiation Field Analysis

Metrics such as field size, penumbra, flatness, and symmetry of the radiation field can be analyzed based on the profiles of the static field image on the EPID, with different calculation protocols in both evaluated tools. In SCM, the image can be manually centered using the graphical interface based on a visible reference. Median filters and profile smoothing are also applied in this step. Once these definitions are set, the following metrics can be calculated: field size, determined at 50% of the profile; penumbra size, measured from 80% to 20% of the profile; flatness assessed using the variance method (Equation 1); and symmetry, evaluated based on the area method (Equation 2)

$$Flatness = 100 \times \frac{D_{max} - D_{min}}{D_{max} + D_{min}} \quad (1)$$

$$Symmetry = 100 \times \frac{A_L - A_R}{A_L + A_R} \quad (2)$$

Where D_{max} is the highest profile value within the field width (up to 80%) and D_{min} is the lowest value within the field width. The area to the left of the CAX up to 80% of the profile is designated as A_L, and similarly, A_R represents the right side.

In the field analysis module of Pylinac, it is also possible to apply a median filter by specifying the number of neighboring pixels for the filter. In this case, a median filter of size three was applied. The same formalisms adopted in SCM were used for calculating penumbra, flatness, and symmetry. The difference lies in the field size detection method. In addition to the conventional method based on FWHM, Pylinac also allows the use of the inflection method, which is based on the zero-crossing of the second derivative of the profile. This method is recommended when analyzing high-resolution images, such as those from the EPID.

2.2.5. CBCT Analysis

From the images obtained using the Catphan® 604 (The Phantom Laboratory, Salem, NY, USA) phantom, it was possible to perform analyses of the key metrics referenced in the AAPM Task Group 142 report [1] regarding CBCT image quality. These include geometric distortion, spatial resolution, contrast, HU constancy, uniformity, and noise. In addition to those mentioned in the reference, low-contrast visibility and slice thickness of the reconstruction were also measured.

The first step, in both tools, is based on identifying the phantom's modules, as incorrect ROI (Region of Interest) positioning can compromise automatic analysis. Therefore, verifying whether the ROIs have been correctly placed via automatic module detection is essential. In SCM, there is a registration interface (Figure 10), where the ROIs can be manually adjusted, along with features for image windowing, magnification, and comparison with a reference image. In the Pylinac CatPhan module, automatic ROI positioning is achieved by identifying the center of the scan section 2 linearity module, and it can detect any rotation of the phantom. The ROIs can be adjusted across all modules or a single specific module, with manual input for position, angle, and scale adjustments.

Figure 10: CBCT image registration interface in SCM. In each of the modules it is possible to adjust the position and angle of the ROI models.

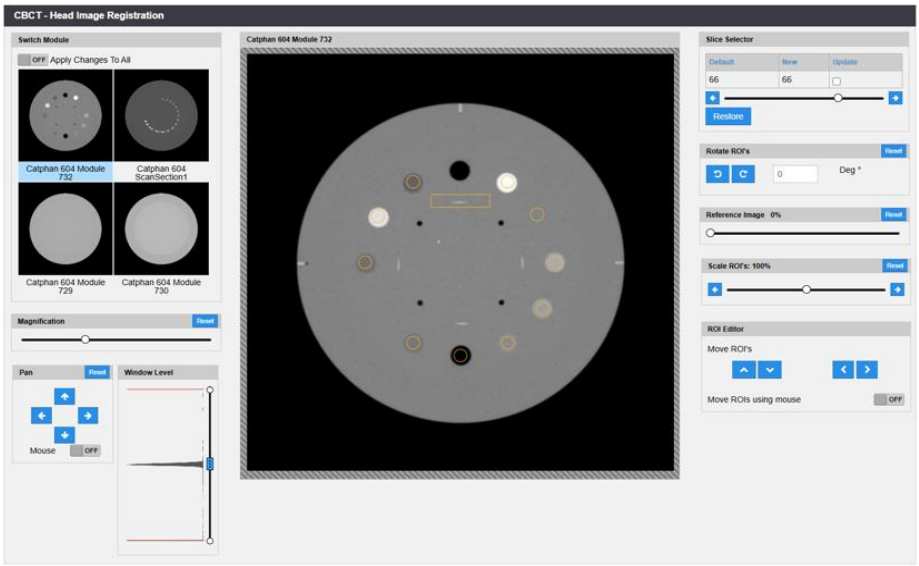

In scan section 1, which contains aluminum inserts with patterns ranging from 1 to 15 line pairs per cm, the evaluation of spatial resolution is performed by calculating the MTF (Modulation Transfer Function). In both tools, spatial resolution was conservatively taken as the value at 50% of the MTF (some references consider the resolution limit at 10% of the MTF [27]).

In scan section 2, geometric distortion, HU linearity, and reconstruction thickness can be evaluated. Geometric distortion is calculated based on four holes whose centers are 50 mm apart. In both tools, the distances between pairs of these holes are calculated, and the maximum absolute difference found in relation to the expected value is reported as geometric distortion. For the HU linearity test, different materials contained in this module are used, and the measured HU value is compared with the nominal expected value (average of the range provided in the simulator object manual). In each material, circular ROIs are evaluated, with SCM taking the mean HU value and Pylinac taking the median value. The maximum difference from the nominal values is computed. Slice thickness is evaluated using two pairs of wires inclined at 23° relative to the base of the phantom. In SCM, the full width at half

maximum (FWHM) of the ROI positioned on the wire is measured and multiplied by the factor given by the tangent of the angle. The same formalism is also used in Pylinac, however, to avoid fluctuations due to noise in the image, an average FWHM value is taken from neighboring slices. Three slices were used for the calculation.

Scan section 3 contains low-contrast targets, with the number of structures visible at the 1% contrast level being evaluated. In SCM, it is assumed that the product of contrast and the ROI diameter remains constant. The visibility criterion for the smallest structure is that the mean ROI value of the structure minus the background mean value must be greater than four times the standard deviation. Visibility in Pylinac is calculated using the signal-to-noise ratio (SNR) based on Rose's criterion [28].

Finally, in scan section 4, uniformity is evaluated based on five ROIs: one central and four at the cardinal angles. SCM calculates uniformity as the maximum difference found between the mean values of a peripheral ROI and the central ROI. In Pylinac, despite using a similar ROI definition, the uniformity index is calculated according to Elstrom's formalism [29]. For comparison purposes, uniformity was also calculated using the SCM method. In this same module, noise is assessed. SCM calculates noise as the standard deviation in HU within the ROI, while Pylinac calculates the average Noise Power, obtaining noise dependence on frequency through the 2D Fourier transform of the image [27].

3. RESULTS AND DISCUSSIONS

Table 2 presents the main results obtained for each of the tests in the analyses performed using SCM and the implemented modules of Pylinac. The adopted tolerances, based on the correspondence of the obtained quantities with those from reference documents, are also presented together. As shown, both interfaces can calculate the

quantities of interest in the reference documents related to the tests carried out, and the values found are within the expected tolerances.

Table 2: Results obtained in the tests analyzed in the SCM, in the Pylinac modules, and tolerance based on the reference documents

Test	Measurement	SCM	*Pylinac*	Tolerance
Picket Fence	Maximum leaf gap position error (mm)	0.16	0.12	0.5[a]
	Minimun leaf gap position error (mm)	0.00	-	-
	Mean leaf gap position error (mm)	0.00	0.03	-
	Mean leaf gap width (mm)	15	15	-
	σ of leaf gap possition error (mm)	0.05	-	-
	σ of leaf gap width error (mm)	0.05	-	-
	MLC Skew (°)	-	0.02	-
Star Shot	Inscribed circle diameter Gantry (mm)	0.53	0.50	2[a]
	Inscribed circle diameter Collimator (mm)	0.14	0.16	2[a]
	Inscribed circle diameter Couch (mm)	0.50	0.48	2[a]
Winston - Lutz	Maximum deviation 2D (mm)	0.83	0.85	2[b]
	Mean deviation 2D (mm)	-	0.65	-
	Modulus of the optimal shift vector (mm)	0.16	0.24	1
	Gantry isocenter diameter 3D (mm)	0.62	0.53	2[a]
	Collimator isocenter diameter 2D (mm)	-	0.2	2[a]
	Couch isocenter diameter 2D (mm)	1.41	1.47	2[a]
	Maximum EPID RMS deviation (mm)	-	0.27	-
Field Analysis	Radiation size Y (cm)	9.93	9.94	9.8-10.2
	Radiation size X (cm)	9.85	9.91	9.8-10.2
	Deviation light/radiation Y (mm)	-0.7	-0.6	±2
	Deviation light/radiation X (mm)	-1.5	-0.9	±2
	Flatness Y (%)	1.85	1.83	±2% *baseline*
	Flatness X (%)	1.88	1.83	±2% *baseline*
	Symmetry Y (%)	0.83	-0.69	±2% *baseline*
	Symmetry X (%)	0.62	-0.62	±2% *baseline*
	Greater penumbra width (mm)	4.0	4.1	-
CBCT	Geometric distortion (mm)	0.28	0.23	≤ 1
	Spatial resolution (mm)	1.61	1.67	≤ 2[c]

Test	Measurement	SCM	*Pylinac*	Tolerance
CBCT	Contrast	0.95	-	≥ *baseline*
	Low Contrast	-	0.35	-
	Low contrast dectability (mm)	4	5	≤ *baseline* [c]
	HU Constancy – Maximum deviation (HU)	21	22	±40
	Noise (HU)	2.72	0.17	≤ *baseline*
	Uniformity (HU)	3.93	3.00	≤ *baseline*
	Slice thickness(mm)	2.50	1.93	-

a – Tolerance *AAPM MPPG 8.b: Linear accelerator performance tests* [14].
b - Tolerance *AAPM MPPG 9.a: for SRS/SBRT* [16].
c - Tolerance *AAPM TG 179 - Quality assurance for image-guided radiation therapy utilizing CT-based* [9].
σ – Standard Deviation
baseline: relative to the established baseline
When not specified, references to *AAPM TG 198* [15] tolerances

Table 3 provides comparisons between the evaluated interfaces, highlighting the main functionalities and available tools. In general terms, we would highlight the graphical interfaces present in the SCM for viewing and registering images, as well as functionalities such as automatic image export, test scheduling and historical data trend analysis. These functionalities add value to the interface, making QA's routine easier and faster, as all control is on a single platform. Although these tools can be implemented in Pylinac, they require more development time, since the only ones available natively are automated image analysis and report generation. While pylinac requires considerable development and programming time to unite the modules into a single user-friendly interface, SCM already provides a simple intuitive, and integrated interface for everyone involved in quality control, positively impacting the routine much more quickly. Even with these apparent negative points, it's undeniable how Pylinac makes it possible to make QA's routine more efficient and effective for free, especially for institutions in developing countries with more prohibitive budgets.

Table 3: Comparison of functionalities and tools in SCM interfaces and Pylinac modules.

Test	Functionality	SCM	*Pylinac*
General Aspects	Interactive Graphical Interface	Present	Developable
	Automation and Record	Present	Developable
	Test Schedule	Present	Developable
	Data Trending	Present	Developable
	Customization	Limited to present metrics	Higher customization
	Learning and Facility	Intuitive	Programming Required
Picket Fence	Image Format	DICOM,TIFF, PNG, BMP, JPEG	DICOM
	MLC Identification	Automatic	Automatic
	Visual Interface Leaves	Present	Missing
	Leaf error histogram	Missing	Present
	Export Data *MLC*	Present	Present
Star Shot	Image Format	DICOM, TIFF, PNG, BMP, JPEG	DICOM, TIFF, PNG, BMP, JPEG
	Composite Image	Present	Present
	Adjustment Tool Spoke Shots	Threshold Value	Circular Profile Radius
	Optimal Circle Visualization	Present	Present
Winston-Lutz	Image Format	DICOM	DICOM
	Isocenter Visialization	Missing	Present
	Simulation Virtual Shifting	Partial	Present
	Additional Analysis	Sag, Beam Steering	Separate Components
Field Analysis	Image Format	DICOM,TIFF, PNG, BMP, JPEG	DICOM
	Center Definition	Visual Interface	Automatic / Manual
	Different Analysis Protocols	Present	Present
	View Metrics in Profile	Missing	Present
	Comparison of Previous Profiles	Present	Missing
CBCT	Image Format	DICOM	DICOM
	ROIs Positioning	Automatic	Automatic
	ROIs Adjustment Visual Interface	Present	Missing

3.1. Picket Fence

Among the values found in the Picket Fence test, the lowest maximum leaf position error was observed in the Pylinac module (0.12 mm, compared to 0.16 mm in SCM). This difference is likely due to the method used to identify the leaf position in Pylinac, as it is based on the FWHM center rather than fitting a curve, as done in SCM.

The skew angle provided in the Pylinac module should also be highlighted. Skew is identified when the lines appear thicker at one end than at the other, indicating a possible deviation in the linear motion of the MLC leaf banks. This measurement may be masked by image registration in the SCM interface since the image angle is adjusted to the cardinal position during the registration stage before calculation, and this angle is not subsequently reported. Even so, the skew value reported in the Pylinac Picket Fence module should be interpreted with caution, as it may be influenced by EPID displacement and rotation.

Regarding the interface, the ability to view the analyzed image interactively in SCM (Figure 11) stands out, allowing users to select a specific pair of leaves and quickly check their results. Although simple, this interface enables easy identification of the leaf pair, which is not always as intuitive when only numbers are displayed, as is the case in Pylinac.

Figure 11: Picket Fence Test SCM interface. Each leaf pair can be viewed and selected, providing easy access to each peak of the expected and calculated leaf position.

In terms of results, the histogram of leaf position errors in Pylinac (Figure 12, right) serves as an excellent summary of the results, rather than simply reporting a maximum error value, showing the distribution of leafs position errors found, as well as illustrating the tolerance and action levels provided.

Figure 12: Results of the analysis of the Picket Fence test in Pylinac. On the left, the leaf positions calculated, highlighted in pink those that differ more than 0.1 mm from the expected position. On the right, the histogram of leaf position error, with the pink lines representing the tolerance levels, and the red ones, the action levels.

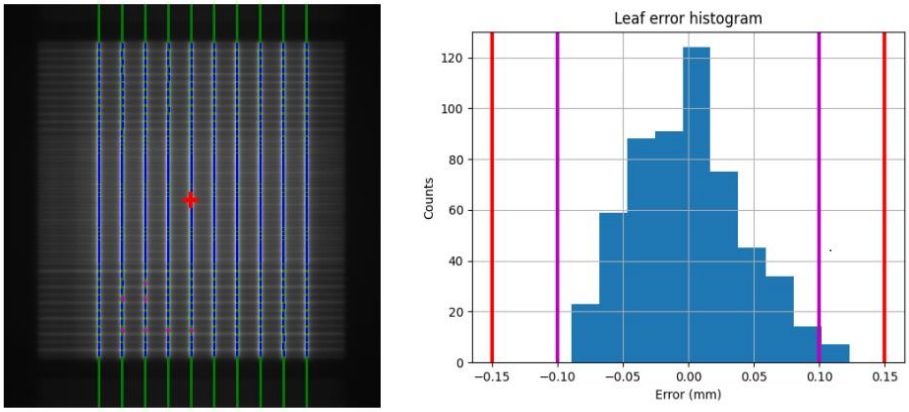

Furthermore, the values obtained using the combined analysis in both tools are consistent, following the stricter criterion suggested by the Report of AAPM MPPG8.b [14] for a quantitative analysis of leaves positions with a tolerance of 0.5 mm. The individual leaf detection method available in Pylinac, despite having advantages in detecting errors in specific situations when well-implemented, tends to be less robust and more prone to errors. This is due to the need to provide the nominal gap value of leaf pairs, which depends on the combined plan gap, the dosimetric leaf gap (DLG), and even EPID scattering effects, thus requiring further studies for proper implementation.

3.2. Star Shot

Regarding the Star Shot test, both tools provide very similar solutions, as well as comparable values for the diameter of the smallest circle inscribed in the lines. However, the

method for identifying spoke shots stands out, particularly in cases where automatic detection fails to correctly identify all the lines, requiring manual parameter adjustments.

In the case of SCM, it is necessary to adjust the gray threshold value in the image registration interface, lowering it only until all spokes are visible and solid within the analysis circumference. Although this adjustment process is rarely needed (in our experience around 15%), it introduces operator subjectivity into the analysis and increases the possibility of errors, as it can significantly alter the final measured value.

In contrast, in Pylinac, this adjustment is made by modifying the radius of the sampled circular profile. Thus, choosing an intermediate radius is sufficient since, at the center, the intensity of the rays tends to overlap, and at the edges, it decreases (especially in images acquired with radiochromic film). Consequently, if images are consistently acquired and processed in the same way, a standard value can be established, minimizing the potential for operator-induced errors. Figure 13 presents the detected spoke shots and the smallest inscribed circle drawn along the lines in both SCM and Pylinac.

Figure 13: Results of the analysis of the Star Shot test, upper SCM, and lower Pylinac. On the left, the spoke shots identified for the composite image of the collimator. On the right, the smallest circle inscribed in the lines found.

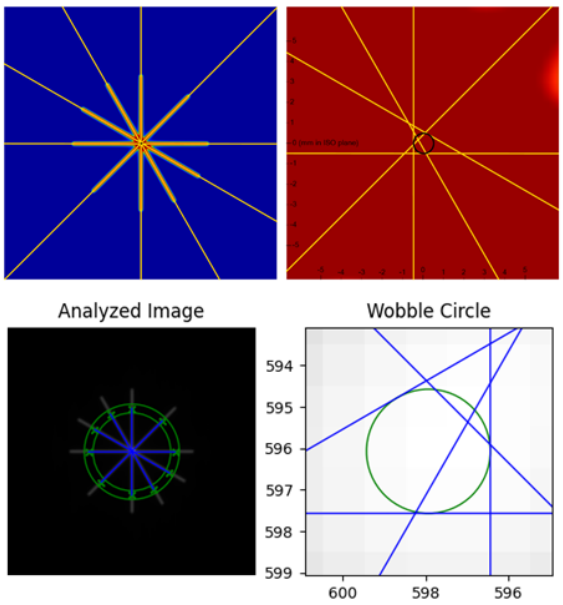

3.3. Winston-Lutz

The results of the 2D analysis of the maximum error found from the center of the field to the radiopaque sphere were similar between the tools, remaining within the 1 mm tolerance. Figure 14 presents the visualization of the identification of the center of the field and center of the sphere in each of the interfaces. Despite being simpler the visualization of the field center and the sphere in SCM images, it is visually easier to verify whether the identification occurred as expected.

Figure 14: Visual identification of the center of radiation field and radiopaque sphere in the Winston-Lutz test on the acquired images. On the left, SCM analysis, where the deviation vector between the centers is shown below the acquired image; on the right, Pylinac analysis, where the center of the EPID is also show.

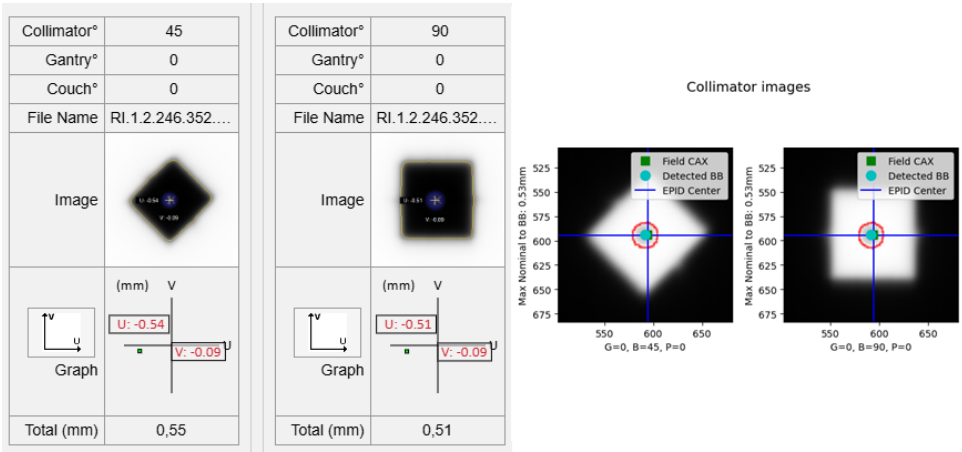

Since the sphere was positioned at the mechanical isocenter of the accelerator, we can interpret the optimal shift vector as a measure of the coincidence between the mechanical and radiation isocenters. Although both results are within the 1 mm tolerance, a notable difference is observed in the modulus of the displacement vector obtained: 0.24 mm in Pylinac and 0.16 mm in SCM, with the latter not providing the necessary shift in the vertical direction.

The virtual shifting tool in Pylinac allows for recalculating the 2D error values by simulating the ideal displacement, without modifying the 3D isocenter values, such as those of the gantry and collimator, since these are calculated independently of the sphere's position.

Figure 15 shows the deviations found in each component as a function of the evaluation axis angle in Pylinac, which helps in the clinical routine to identify which component causes the greatest deviations.

Figure 15: Results of the analysis of the Pylinac Winston-Lutz test, separating the error due to gantry, collimator, table, and EPID.

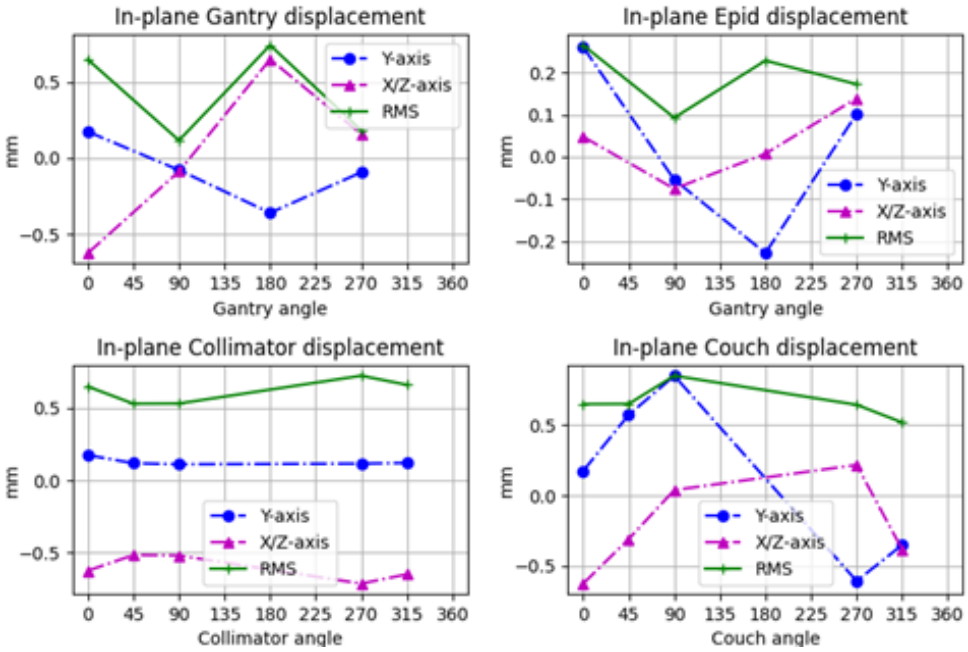

In SCM, an analysis of this type is missing for the collimator and EPID, as it only presents the values for the gantry and couch separately. Additionally, SCM lacks a more robust virtual shifiting tool, as it only demonstrates this graphically and specifically for couch rotations. The additional graphs in SCM, which use the measured data to plot the expected curves for gantry sag (Figure 16) and beam steering errors, provides interesting additional analyses that could help identify deviation trends and adjustment directions. However, they lack detailed methodological documentation to assist in their interpretation.

Figure 16: Gantry sag results based on Winston-Lutz results in SCM. The blue line shows the x-component of the gantry sag, the green line the y-component, and in red the total.

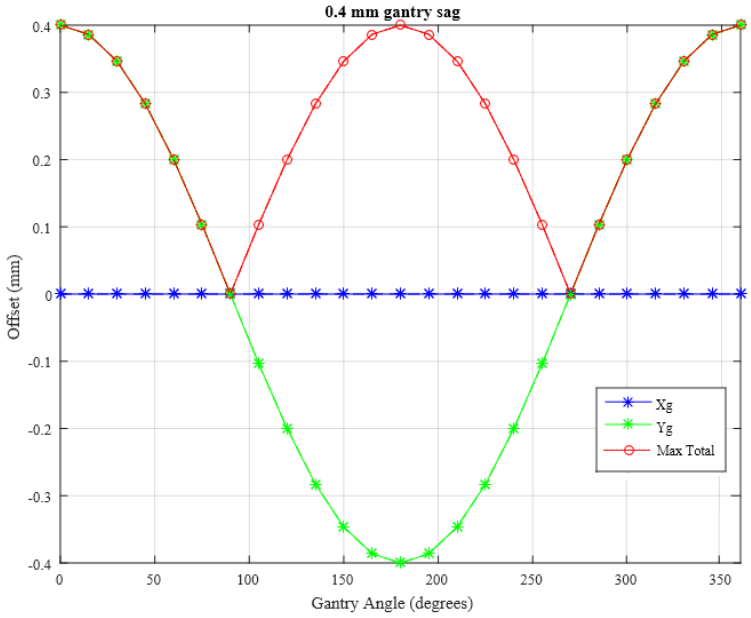

3.4. Field Analysis

Regarding the parameters of the analyzed radiation field, both implementations obtained the relevant quantities with good agreement and within tolerance levels [15]. The use of the radiopaque marker at the center of the light field proved to be a good alternative for establishing a comparison reference with the light field. In SCM, centralization is facilitated by the visual interface, allowing the center to be placed directly on the marker in the image. In contrast, in Pylinac, this process is more challenging, requiring manual adjustments to the centralization parameters, which can then add an unwanted dependent operator process to the analysis if necessary.

For the calculated field size, even with different metrics, similar results were obtained. The ability to determine the field size using the inflection method is an advantage of Pylinac, especially when dealing with FFF (Flattening Filter Free) energy fields, where the FWHM metric is not appropriate.

Regarding profile visualization, Pylinac stands out by displaying the identified field edges, penumbra region, and regions considered for symmetry and flatness calculations (Figure 17). However, it lacks an easy-to-use implementation for comparing two profiles, a feature available in SCM, which aids in periodic result comparisons. This feature can be implemented in Pylinac with programming, requiring more development time

Figure 17: Analyzed radiation field profile and visualization of the chosen metrics in Pylinac

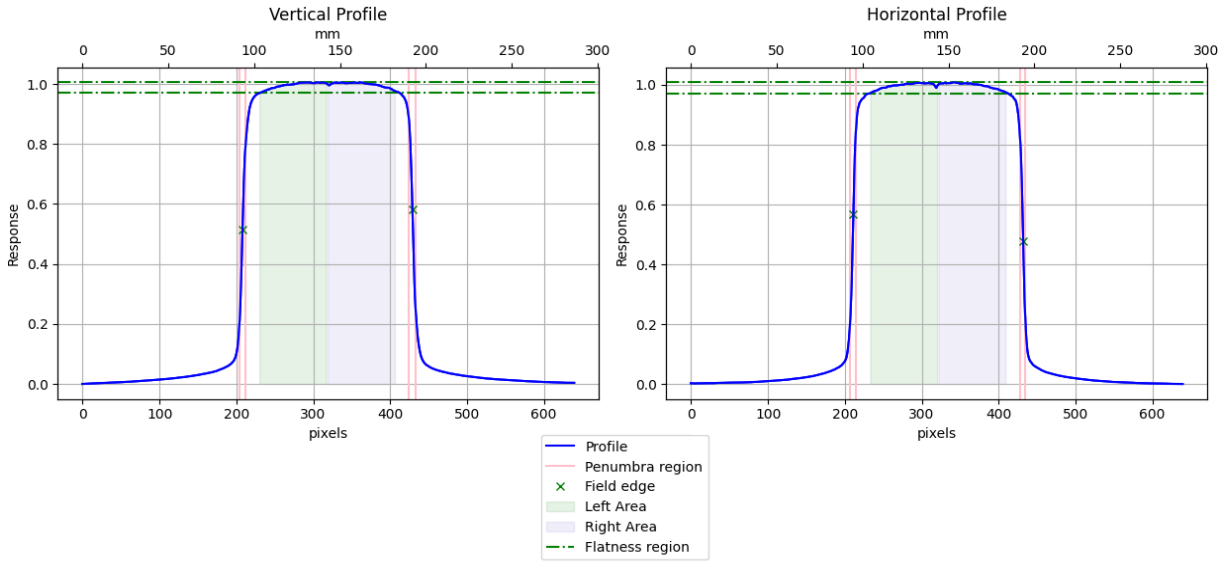

The symmetry and flatness metrics derived from the EPID image proved to be feasible. However, factors that influence the beam profile, such as the central marker and the treatment couch, must be considered. As a result, this method should be used only as a monthly constancy test, provided that the same conditions are maintained. Therefore, it is essential to perform a water tank scan at least annually to obtain symmetry and flatness values and compare them with the machine's acceptance values [15].

3.5. CBCT

In the analysis of CBCT images, the metrics referenced in the literature were evaluated in both tools, however, some differences can be noted. Regarding the analysis ROIs, both implementations performed well in automatic positioning, but the visual interface in SCM attract attention as a clear advantage when adjustments are necessary.

The noise evaluation in Pylinac using the Noise Power Spectrum provides a more detailed analysis compared to the standard deviation method applied to the ROI in SCM. Two ROIs with the same standard deviation value may present very different noise distributions across frequencies. This directly impacts noise perception and can be quantitatively measured through the average value of the Noise Power distribution.

The Pylinac methodology, which uses multiple slices to determine the reconstruction thickness, showed a result closer to the nominal thickness of 2 mm (SCM 2.5 mm and Pylinac 1.93 mm).

Contrast is evaluated differently between the implementations. In SCM, contrast is calculated based on the Teflon insert relative to the background, yielding a value of 0.95. On the other hand, Pylinac assesses contrast using the smallest visible target in module 730, which contains structures with a nominal contrast level of 1%, resulting in a contrast value of 0.35. Since the references do not specify a clear methodology for contrast evaluation, both approaches are valid for establishing a baseline. The SCM method is more straightforward, relying on a high-contrast structure, whereas the Pylinac approach considers a more limiting case based on the visibility of low-contrast structures.

4. CONCLUSIONS

Both automated image analysis interfaces evaluated, the commercial SCM from Sun Nuclear and the web application implemented using modules from the open-source Pylinac library, were able to quantify the relevant metrics in a manner consistent with the reference test documents and meet the service's needs. This contributes to a Quality Assurance Program with reduced image analysis time, lower susceptibility to inter-operator errors, and greater precision and standardization in results, minimizing subjectivity in the process.

The SCM platform, in addition to automated analyses, offers an interactive interface that integrates the entire quality control process, from automated image and log exports to test scheduling, result recording, and trend analysis through graphical representations. This set of tools further enhances the advantages already mentioned, making QA's routine easier and faster, as all control is integrated on a single platform..

The web interface developed using Pylinac modules demonstrated that, even at a basic level, it is possible to create tools similar to commercial solutions using available open-source libraries, allowing for customization to fit the specific needs of a Quality Assurance Program. However, the time investment and challenges involved in its development are undeniable, requiring more time to implement and integrate into a user-friendly interface.

Regardless of the interface used, the role of the medical physicist remains crucial, whether in developing or validating these tools, ensuring a thorough understanding of the algorithms and methodologies used in the analyses, as well as their limitations and critical aspects. When necessary, conducting studies is essential to prevent incorrect tool usage from leading to erroneous quantifications, avoiding potential risks and fostering a safe and efficient Quality Assurance Program.

ACKNOWLEDGMENT

To INRAD and all professionals involved where this study was carried out.

FUNDING

To the Health Ministry (SGTES) and the Ministry of Education (SESu) for the financial support during the residency period.

CONFLICT OF INTEREST

All authors declare that they have no conflicts of interest.

REFERENCES

[1] KLEIN, E. E.; HANLEY, J.; YIN, F. F.; *et al.* Task Group 142 report: Quality assurance of medical accelerators. **Medical Physics**, v. 36, n. 9, p. 4197–4212, 17 set. 2009. DOI: 10.1118/1.3190392.

[2] SAW, C.; FERENCI, M.; WAGNER, J. H. Technical aspects of quality assurance in radiation oncology. **Biomedical Imaging and Intervention Journal**, v. 4, n. 3, jul. 2008. DOI: 10.2349/biij.4.3.e48.

[3] FURNARI, L. (2015). Controle de qualidade em radioterapia. **Revista Brasileira De Física Médica**, v. 3(1), p. 77–90, 2009. DOI: 10.29384/rbfm.2009.v3.n1.p77-90.

[4] CONNELL, P. P.; HELLMAN, S. Advances in Radiotherapy and Implications for the Next Century: A Historical Perspective, **Cancer Research**, v. 69, n. 2, p. 383–392, 15 jan. 2009. DOI: 10.1158/0008-5472.CAN-07-6871.

[5] LUTZ, W.; WINSTON, K. R.; MALEKI, N. A system for stereotactic radiosurgery with a linear accelerator. **International Journal of Radiation Oncology Biology Physics**, v. 14, n. 2, p. 373–381, fev. 1988. DOI: 10.1016/0360-3016(88)90446-4.

[6] WOO, M. K.; O'BRIEN, P.; GILLIES, B.; *et al.* Mechanical and radiation isocenter coincidence: An experience in linear accelerator alignment. **Medical Physics**, v. 19, n. 2, p. 357–359, mar. 1992. DOI: 10.1118/1.596866.

[7] LING, C. C.; ZHANG, P.; ARCHAMBAULT, Y.; *et al.* Commissioning and Quality Assurance of RapidArc Radiotherapy Delivery System. **International Journal of Radiation Oncology Biology Physics**, v. 72, n. 2, p. 575–581, out. 2008. DOI: 10.1016/j.ijrobp.2008.05.060.

[8] BREDIKIN, A. Z.; WALSH, M. J. Dose rate versus gantry speed performance evaluation for slow gantry speeds using DICOM RT plans. **Journal of Applied Clinical Medical Physics**, v. 23, n. 10, 19 out. 2022. DOI: 10.1002/acm2.13786.

[9] BISSONNETTE, J.; BALTER, P. A.; DONG, L., *et al.* Quality assurance for image-guided radiation therapy utilizing CT-based technologies: A report of the AAPM TG-179, **Medical Physics**, v. 39, n. 4, p. 1946–1963, 20 abr. 2012. DOI: 10.1118/1.3690466.

[10] STAMBAUGH, C.; YANCEY, J.; SHUKLA, U.; *et al.* Daily Quality Assurance Efficiency Evaluation Using SunCHECK Machine and Machine Performance Check. **Cureus**, 2 mar. 2023. DOI: 10.7759/cureus.35695.

[11] DHOUNDIYAL, M.; RASAL, S.; GUPTE, A.; *et al.* Validation and Efficiency Evaluation of Automated Quality Assurance Software SunCHECK™ Machine for Mechanical and Dosimetric Quality Assurance. **Journal of Medical Physics**, v. 49, n. 2, p. 311–315, abr. 2024. DOI: 10.4103/jmp.jmp_158_23.

[12] BONANNO, E.; BORZÌ, G. R.; CAVALLI, N.; *et al.* Use of an automated software module for monthly routine Machine QA tests. **Journal of Instrumentation**, v. 18, n. 07, p. T07010, 1 jul. 2023. DOI: 10.1088/1748-0221/18/07/T07010.

[13] KERNS, J. R. Pylinac: Image analysis for routine quality assurance in radiotherapy. **Journal of Open Source Software**, v. 8, n. 92, p. 6001, 3 dez. 2023. DOI: 10.21105/joss.06001.

[14] KRAUSS, R. F.; BALIK, S.; CIRINO, E. T.; *et al.* AAPM Medical Physics Practice Guideline 8.b: Linear accelerator performance tests. **Journal of Applied Clinical Medical Physics**, v. 24, n. 11, 1 nov. 2023a. DOI: 10.1002/acm2.14160.

[15] HANLEY, J.; DRESSER, S.; SIMON, W.; *et al.* AAPM Task Group 198 Report: An implementation guide for TG 142 quality assurance of medical accelerators. **Medical Physics**, v. 48, n. 10, 11 out. 2021. DOI: 10.1002/mp.14992.

[16] HALVORSEN, P. H.; CIRINO, E.; DAS, I. J.; *et al.* Medical Physics Practice Guideline 9.a. for SRS/SBRT. **Journal of Applied Clinical Medical Physics**, v. 18, n. 5, p. 10–21, 8 set. 2017. DOI: 10.1002/acm2.12146.

[17] Phantom Laboratory Incorporated. Catphan ® 604 Manual. Salem, NY, USA, 2015.

[18] LIM, R.; PECONONCELLO, G. P; HOBBIS, D.; *et al.* Technical note: Characterization of novel iterative reconstructed cone beam CT images for dose tracking and adaptive radiotherapy on L-shape linacs. **Medical Physics**, v.49, n. 12, p 7715-7732, dez. 2022. DOI: 10.1002/mp.15943.

[19] SunCHECK® Machine Reference Guide. Sun Nuclear, Melbourne, FL, USA, 2024.

[20] Streamlit library. Available at: https://docs.streamlit.io/. Accessed on: April 6,2025

[21] MAMALUI-HUNTER, M.; LI, H.; LOW, D. A. MLC quality assurance using EPID: A fitting technique with subpixel precision. **Medical Physics**, v. 35, n. 6Part1, p. 2347–2355, 19 jun. 2008. DOI: 10.1118/1.2919560.

[22] GONZÁLEZ, A.; CASTRO, I.; MARTÍNEZ, J. A. A procedure to determine the radiation isocenter size in a linear accelerator. **Medical Physics**, v. 31, n. 6, p. 1489–1493, 24 jun. 2004. DOI: 10.1118/1.1755491.

[23] DEPUYDT, T.; PENNE, R.; VERELLEN, D.; *et al.* Computer-aided analysis of star shot films for high-accuracy radiation therapy treatment units. **Physics in Medicine and Biology**, v. 57, n. 10, p. 2997–3011, 21 maio 2012. DOI: 10.1088/0031-9155/57/10/2997.

[24] LOW, D. A.; LI, Z.; DRZYMALA, R. E. Minimization of target positioning error in accelerator-based radiosurgery. **Medical Physics**, v. 22, n. 4, p. 443–448, 4 abr. 1995. DOI: 10.1118/1.597475.

[25] WINKLER, P.; BERGMANN, H.; STUECKLSCHWEIGER, G.; *et al.* Introducing a system for automated control of rotation axes, collimator and laser adjustment for a medical linear accelerator. **Physics in Medicine and Biology**, v. 48, n. 9, p. 1123–1132, 7 maio 2003. DOI: 10.1088/0031-9155/48/9/303.

[26] HANCOCK, S.; HYER, D.; NIXON, E. SU-E-T-54: A New Method for Optimizing Radiation Isocenter for Linac-Based SRS. **Medical Physics**, v. 42, n. 6Part12, p. 3343–3343, 29 jun. 2015. DOI: 10.1118/1.4924415.

[27] BUSHBERG, J. T.; SEIBERT, J. A.; LEIDHOLDT, E. M.; *et al.* **The Essential Physics of Medical Imaging**. Philadelphia, PA, US: Lippincott Williams and Wilkins (3Ed), 2012. ISBN 978-0-7817-8057-5

[28] ROSE, A. The Sensitivity Performance of the Human Eye on an Absolute Scale. **Journal of the Optical Society of America**, v. 38, n. 2, p. 196, 1 fev. 1948. DOI: 10.1364/JOSA.38.000196.

[29] ELSTRØM, U. V.; MUREN, L. P.; PETERSEN, J. B. B.; *et al.* Evaluation of image quality for different kV cone-beam CT acquisition and reconstruction methods in the head and neck region. **Acta Oncologica**, v. 50, n. 6, p. 908–917, 18 ago. 2011. DOI: 10.3109/0284186X.2011.590525.

LICENSE